Physica B 460 (2015) 218–221

Contents lists available at ScienceDirect

Physica B

journal homepage: www.elsevier.com/locate/physb

Spin and charge order in Hg1201

G. Nikšić *, D.K. Sunko, S. Barišić

Department of Physics, Faculty of Science, University of Zagreb, Bijenička 32, 10000 Zagreb, Croatia

ARTICLE INFO

Available online 24 November 2014

Keywords:
High T_c
Cuprates
Antiferromagnetism
Pseudogap
Neutron scattering

ABSTRACT

We describe the Hg1201 cuprate in the pseudogap (PG) phase from a 3-band Fermi liquid point of view. The PG is modeled by a k-dependent gap parameter $\Delta(k)$, conforming with experiment. Susceptibilities are evaluated in the low-temperature metallic state without further renormalisation by interactions. The effect of strong correlations in the 2D metal is studied by coherent kinematic factors, originating from setting the Hubbard $U_d \to \infty$ [1].

The magnetic susceptibility shows a Y-shaped transverse spin response much like the recent experimental results [2] in the PG phase of Hg1201. The response is suppressed below the commensurate peak at $\omega = 2\Delta_0$. The strongly anisotropic gap $\Delta(k)$ extends the non-dispersive vertical part of the Y-shape, as seen in experiment. (Using an isotropic gap yields a very short vertical part, making the response more V-shaped.) At higher frequencies it displays isotropic upward branches from interband excitations.

The SDW gap $\Delta(k)$, assumed to open at $T^* \approx 300$ K, reconstructs the Fermi surface, leaving only a pocket around the nodal points. The bands at $T_{CDW} \ll T^*$nest to give a q_{CDW} of around 0.28 r.l.u., as observed [3]. Such a gapped Fermi liquid scenario suffices to understand the charge and spin responses of underdoped Hg1201 in the experimentally observed hierarchy. The kinematic correlations caused by a large U_d change the Y-response towards the "hourglass" X-shape, thus replacing the peak at $\omega = 2\Delta_0$ and $q = \mathbf{Q}_{AF}$ with incommensurate downward branches. This result indicates that effects of strong-coupling correlations at the Fermi surface are more significant in the lanthanum than in the mercury cuprates.

1. Introduction

The cuprate high-temperature superconductors (HTSC) present the foremost unsolved problem in condensed matter physics. Apart from the SC mechanism, the so-called pseudogap (PG) has received much attention, because it is believed to hold the key to the understanding of the metallic state apart from SC. One important feature of the PG is the strongly **k**-dependent pseudogap function along the Fermi surface, strikingly different from a simple d-wave: it is maximal at the antinode and vanishes in a wide range of wave-vectors around the node, the Fermi-surface arc. This signature of the PG phase is observed in all cuprates where it has been measured. The Kerr effect points to the magnetic origin of the pseudogap [4,5]. Recent experiments [6] have shown that the length of the Fermi arc and the size of the gap appearing around the antinodes at the pseudogap temperature T^* can be directly manipulated by extrinsic (out-of-plane) disorder. This observation opens the possibility that the PG is not an intrinsic feature of the 2D carriers in the copper-oxide planes. The present calculations are not sensitive to the origin of the gap, as parametrized from experiments.

Here we focus on the most recent experiments on the paradigmatic single-plane cuprate $HgBa_2CuO_{4+\delta}$ (Hg1201), and comment on the other classes of cuprates. Inelastic neutron scattering (INS) [2] in Hg1201 uncovers a magnetic excitation spectrum, visually resembling a wine glass, as opposed to the "hourglass" shape seen e.g. in LSCO and YBCO. It consists of a vertical non-dispersive branch, appearing above 20 meV, and a high-energy isotropic dispersive branch, connecting at a pronounced peak at 60 meV. We identify these high-energy branches as interband particle-hole excitations above the gap, the commensurate peak being their crossing point, i.e. the lowest possible energy at which a significant number of ph pairs can be excited at $\mathbf{q} = \mathbf{Q}_{AF}$. All excitations below the gap are at least partially suppressed, even if the gap is not constant over the BZ. The edge of the Fermi arc is also the point whose nesting in the intraband channel generates the CDW peak around 0.28 r.l.u., as seen in RIXS [3].

We have observed all of the above-mentioned features in Im $\overline{\chi}^0$, i.e. the effectively non-interacting susceptibility below the PG temperature T^*. The experimentally measured gap we impose in our 2D approach allows us to correctly reproduce the observed neutron spectra and CDW vectors. Since all of the experimental

* Corresponding author.
E-mail addresses: gniksic@phy.hr (G. Nikšić), dks@phy.hr (D.K. Sunko), sbarisic@phy.hr (S. Barišić).

http://dx.doi.org/10.1016/j.physb.2014.11.075
0921-4526/

features at $\mathbf{q} = \mathbf{Q}_{AF}$ are essentially insensitive to the SC transition [2], we do not consider the SC channel here.

2. Model

The bare band used here is the conduction band of the non-interacting Emery three-band model. The microscopic parameters are two hopping integrals t_{pd} and $t_{pp} < 0$ and the energy gap between bare orbital energies Δ_{pd}. One would require at least a fourth orbital (copper 4 s) in order to keep all parameters' values chemically correct, but three are sufficient here, at the price of a phenomenologically large value of t_{pp}, as a consequence of this downfolding [7]. The parameters are set so that they roughly fit the dispersion slope at the node, and the chemical potential is set manually for any gap magnitude to yield a doping of around 10% holes, with $T \approx 100$ K.

The on-site repulsion $U_d \to \infty$ induces a kinematic correlation, because a hole jumping onto a copper d orbital has to wait for the previous one to leave it. As described elsewhere [1], this modifies the spectral weight of propagators, introducing a multiplicative factor in the susceptibilities. These factors are included in our pseudogap scenario in a way which respects the symmetry of the gapped state. As shown previously [8], these correlations ensure that any transition at T^* is necessarily commensurate.

The gap is taken to open in a way similar to the (antiferro) magnetic spin-Peierls model, as widely used in the literature, but with the gap as an extrinsic property requiring no self-consistency. We assume that it opens around 300 K, splitting the single bonding band into two sub-bands, via an AF $\mathbf{Q} = (\pi, \pi)$ scattering, leaving parts of the Fermi surface ungapped, as in the hole-doped CDW models [9]. We use a simple parametrisation of the gap function:

$$\Delta_{\mathbf{k}} = \frac{\Delta_0}{2^n}\left(\cos k_x a - \cos k_y a\right)^n, \quad n \text{ even.}$$

Band dispersions (Figs. 1 and 2) are obtained by a 2×2 unitary transformation matrix and are given by

$$E_{P,M} = \frac{E_{\mathbf{k}} + E_{\mathbf{k}+\mathbf{Q}}}{2} \pm \sqrt{\left(\frac{E_{\mathbf{k}} - E_{\mathbf{k}+\mathbf{Q}}}{2}\right)^2 + \Delta_{\mathbf{k}}^2},$$

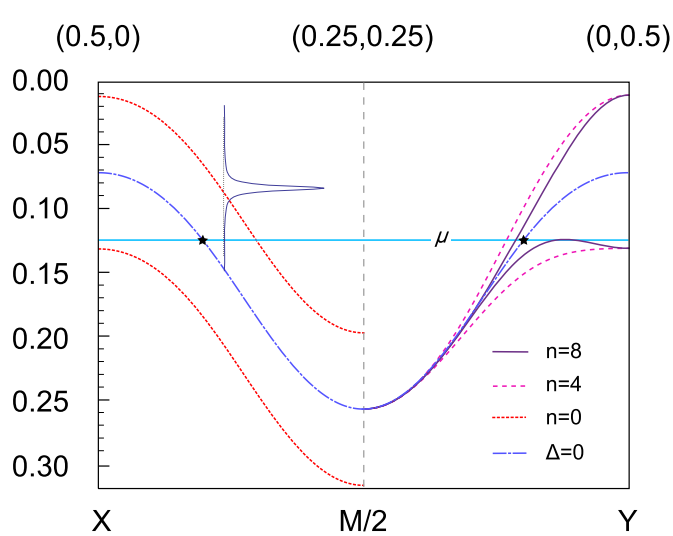

Fig. 1. The band dispersions along the antidiagonal. Left: the bare band and the two bands split by a constant gap (usual AF scenario). The **k** shift of the FS from the hotspot (black stars) is large. Right: the bands for $n=4,8$ with a visible back-bend for $n=8$ and a smaller FS shift from the hotspot. The Lorentzian inset displays the average width of the propagators used.

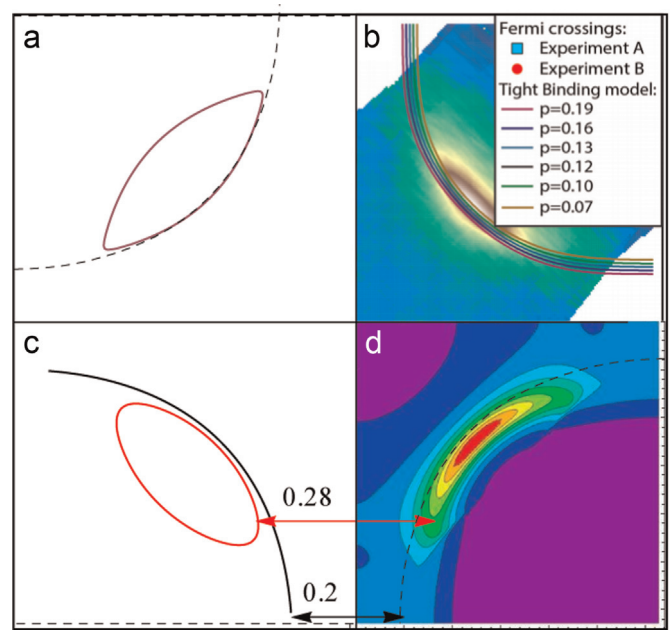

Fig. 2. The Fermi surfaces: (a) for an $n=4$ gap function at 10% doping; (b) FS seen in ARPES in the SC state for the optimally doped Hg1201 (taken from ref. [12]); (c) FS for a constant gap function (red) and the normal state bonding band (black). The gap used is (d) is just large enough to suppress the FS part around the AN. The black and red arrow indicates the best intraband CDW nesting vector available for the non-gapped and gapped states, respectively. (For interpretation of the references to color in this figure caption, the reader is referred to the web version of this article.)

and the eigenvectors (elements of the same unitary matrix) are then used to express the elementary propagator weights and coherent factors $m^{LL'}_{\sigma\sigma'}(\mathbf{k}, \mathbf{k}+\mathbf{q})$ for susceptibilities, which now have 2 interband and 2 intraband contributions. Without going into details, we note that setting $t_{pp} \neq 0$ complicates the expressions from the usual first-neighbour single-band AF approaches, where the dispersions are $\pm\sqrt{E_{\mathbf{k}} + \Delta^2}$ because the next-nearest neighbour hopping $t' = 0$ implies $E_{\mathbf{k}+\mathbf{Q}} = -E_{\mathbf{k}}$.

Since the PG involves no long-range order (LRO), we do not resum the susceptibility below T^* [10,11]. Rather, we extract the magnetic *ph*-excitation spectrum from the peaks in Im $\bar{\chi}^0(\mathbf{q}, \omega)$ in the gapped state:

$$\bar{\chi}^0_{\sigma\sigma'}(\mathbf{q}, \mathrm{i}\omega_m) = \sum_{LL',\mathbf{k}} \left|m^{LL'}_{\sigma\sigma'}(\mathbf{k}, \mathbf{q})\right|^2 \frac{f_{L\mathbf{k}+\mathbf{q}} - f_{L'\mathbf{k}}}{\mathrm{i}\hbar\omega_m - E_{L\mathbf{k}+\mathbf{q}} + E_{L'\mathbf{k}}}$$

After analytical continuation ($\mathrm{i}\hbar\omega_m \to \hbar\omega + \mathrm{i}\eta$), the damping η becomes another important physical parameter (broadening of the fermion spectral functions) which we use to simulate the *pseudo*gap nature of the state. The Fermi surface we set to reproduce is the one seen in ARPES (Fig. 2b). We find that for a realistic FS map (Fig. 2d), one requires a **k**-dependent damping (effectively, the self-energy needs to be self-consistent, even if the gap is not), but for susceptibilities it is enough to keep η constant, between 5 and 50 meV.

3. Results, constant gap

Selecting $n=0$ in our gap function with a 0.001 eV damping η, we recover the usual AF gap scenario: all spectral weight at $\mathbf{q} = \mathbf{Q}_{AF}$ is suppressed below the "resonance" peak at $\omega = 2\Delta_0$, as all filled states in the lower band are exactly $2\Delta_0$ below the upper band (Fig. 3) at (π, π) momentum transfer. Above the peak, an almost parabolic dispersion in the interband channel is recovered, resembling the body of a wine glass, but without the stem seen in

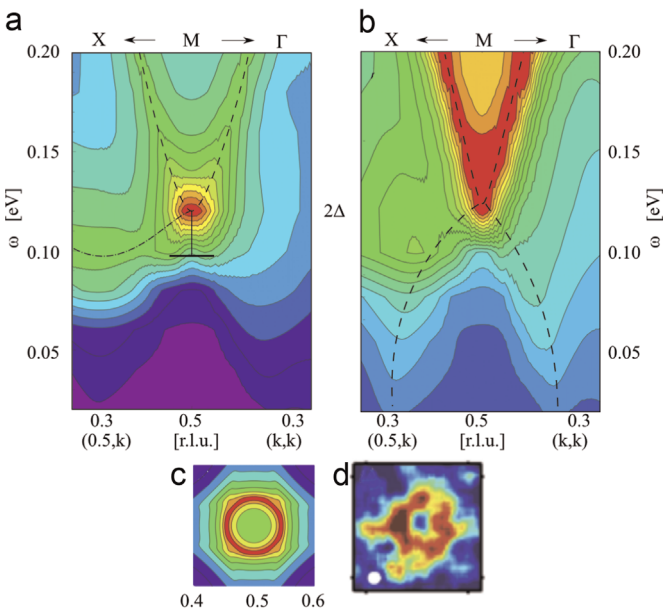

Fig. 3. Im $\overline{\chi}_0(\mathbf{q}, \omega)$ for $n=0$ (constant gap) along 2 high-symmetry lines in the BZ: (a) without strong-correlation effects (cf. experimental results from ref. [2], also on Fig. 5; (b) the same, with the spectral weights originating in kinematic correlations. There is an overall scaling factor of the order 2 with respect to the experiment. Dashed lines are guides to the eye for the interband excitations, dot-dashed for intraband. (c) and (d) Cuts at constant $\omega > 2\Delta$ in our work and in experiment [2], respectively, in the same scale of wave vectors and with the same scaling factor.

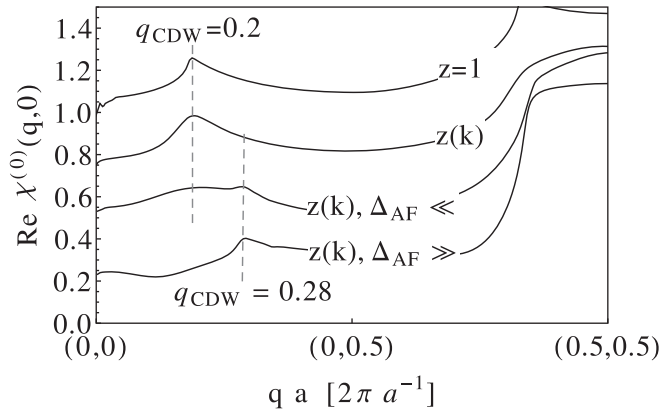

Fig. 4. The real part of the amplitude susceptibility above and below T^*, with potential CDW instability wave vectors of 0.2 and 0.28 r.l.u., respectively. The curves are offset vertically. From top to bottom: (a) Re χ^0 without the gap or correlations; (b) without the gap, with correlations (note the SDW peak becomes *commensurate* as described previously [8]); (c) small gap for $T \lesssim T^*$ (two intraband peaks from two bands, not well distinguished) and (d) large gap, the small FS around the vH point is suppressed and only one strong intraband peak exists, identified with the one from ref. [3].

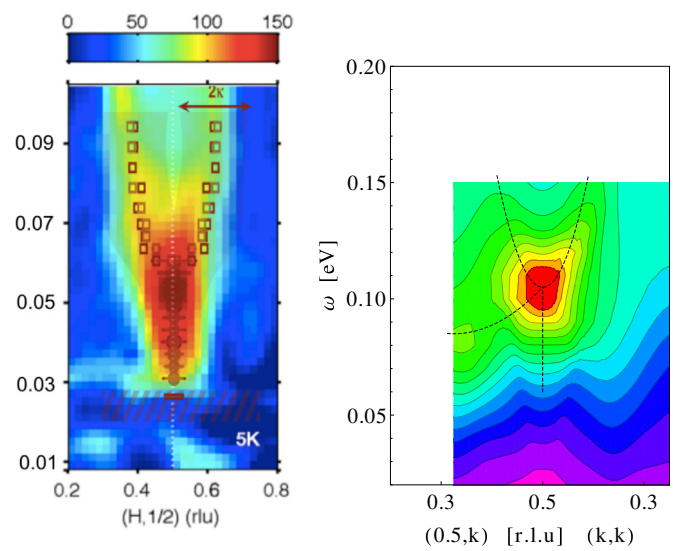

Fig. 5. Im $\overline{\chi}_0$ in the gapped state: (a) experimental spectrum; (b) $n=4$ **k**-dependent gap with a 5 meV damping, fitting the experiment the best way, up to a scaling factor, smaller than the one in Fig. 3.

INS. The parabolic branch would extend all the way to $\omega=0$ in the ungapped state. A weaker intraband dispersion is found along the *X–M* direction, corresponding to the low energy feature, barely visible in the experiment [2]. A wave-vector map at constant $\omega > 2\Delta_0$ reveals a continuum of isotropic magnetic excitations (Fig. 3) forming the bowl of the glass, corresponding nicely to the experimentally observed nearly circular excitation spectrum.

An increase in damping expands the energy intervals in which states can scatter between bands at $\mathbf{q} = \mathbf{Q}_{\mathbf{AF}}$, so that the *ph* excitation strength is no longer strictly bounded by $2\Delta_0$ from below. However, this extends the vertical part of the excitation spectrum (the stem of the "wine glass") only slightly. It takes an unrealistically high η to reproduce the spectrum seen in experiment [2] i.e. suppress the stem of the wine-glass sufficiently at low ω.

Although the incommensurate branches below $\omega = 2\Delta$ are suppressed by the gap, the modified spectral weights due to strong correlations enhance them with respect to the commensurate peak. This recovers the hourglass shape (Fig. 3b) even for this Fermi surface parametrisation, otherwise characteristic for materials without the hourglass.

The amplitude susceptibility (CDW channel) above and below T^* is shown in Fig. 4. After the gap opens, the CDW peak shifts to a higher value, around 0.28 of the BZ, as seen in RIXS [3]. This peak originates in intraband nesting of the oval shaped Fermi surfaces from Fig. 2, where Fermi velocities are parallel. In an ungapped scenario, the same condition is met only at the edge of the BZ, with a smaller wave vector of 0.2 BZ. Both situations are illustrated in Fig. 2.

4. k-Dependent gap and damping effects

For a moderate **k**-dependence ($n=4$) and damping ($\eta=5$ meV) we find the regime that best describes experimental results, even without fitting all numerical parameters to ARPES perfectly. The scaling factor is reduced, because there is now a continuum of (π, π) excitations which reduces the commensurate peak from $2\Delta_0$ to $\omega_{\text{peak}} \approx 0.75 \times 2\Delta_0$. Overdamping suppresses all the features into the continuum of background excitations. Underdamping with abrupt ($n=8$) gaps makes all of the features too pronounced, and the excitations in a narrow interval of $\omega \lesssim 2\omega_{\text{peak}}$ even begin to resemble part of the hourglass dispersion.

For strongly **k**-dependent gaps the FS follows its ungapped shape around the node, and therefore one would require a large pseudogap maximum parameter Δ_0 to shift the CDW peak originating in intraband nesting to a realistic value. It is worthwhile noting that our approach so far only includes the real part of the fermion self-energy which splits the bands with a gap. Simulating the imaginary part with **k**-dependent damping shifts this CDW peak to a higher value than expected from simple nesting and suppresses the Fermi surface reconstruction around the antinodal point. This indicates that, within this approach, it should be possible to find a parameter regime exactly fitting the FS, nodal slope

and pseudogap hump in ARPES, the CDW wave vector seen in RIXS, and the wine glass spectrum from the INS without any scaling factors. It implies that, while the *gap* is not to be treated self-consistently, possibly because it is extrinsic, the *self-energy* should be, because it is induced in the 2D nodal Fermi liquid below the gap.

5. Conclusion: detecting experimental regimes

We have demonstrated a simple model which correctly identifies the scales observed in neutron and X-ray scattering experiments on Hg1201. Taking only the Fermi arc shape and the gap function from ARPES in cuprates as a starting point, we extract experimental spectra and nesting vectors from the effective low-temperature susceptibility $\overline{\chi}^0$, with $T^* > T_{CDW}(> T_C)$. Our model obtains the isotropic "wine glass" Y-shaped spectrum as *ph* interband excitations, without the need to invoke magnons from localised spins. The isotropy of the high-energy part of the cuprates' magnetic spectrum seems to be universal [13], which may prove to be an important constraint for further research into its provenance.

With respect to the shape of the spectrum and the effect of correlations, we suggest that cuprates can be roughly split in two classes. The itinerant carriers in Hg1201, along with YBCO and BSCCO, exhibit the "wine glass" magnetic scattering around the AF vector $\mathbf{Q}_{AF}$, originating from interband excitations of ungapped states from the Fermi arcs. In these materials, the arcs are shorter, oxygen-dominated, and thus less susceptible to strong correlation effects on copper sites. Their nesting triggers a CDW with $T_{CDW} < T^*$. The other class, principally represented by the lanthanum cuprates, features a long Fermi arc, extending almost to the edge of the BZ, and strong downwards-dispersing (hourglass) magnetic excitations. Their charge order is physically different [14], with $T_{CDW} > T_{SDW}$. We identify the lower branches of the hourglass as weak, suppressed interband excitations below the pseudogap, which we show are strengthened by a more sharply **k**-dependent gap and the kinematic effect of strong correlations. The latter are naturally pronounced because more states near the copper-dominated vH points are available at the Fermi level.

We have simulated the self-consistency of the fermionic self-energy by introducing a **k**-dependent damping increasing with the gap. We found that it improves the FS maps in the BZ alongside the magnetic excitation spectra, which we leave for future work.

Acknowledgements

Discussions with I. Kupčić and O. S. Barišić are gratefully acknowledged. This work was supported by the Croatian Government under Project no. 119-1191458-0512 and by the University of Zagreb Grant no. 202301-202353.

References

[1] O.S. Barišić, S. Barišić, J. Supercond. Nov. Magn. 25 (2012) 669–676 (and references therein).
[2] M.K. Chan, C.J. Dorow, L. Mangin-Thro, Y. Tang, Y. Ge, M.J. Veit, X. Zhao, A.D. Christianson, J.T. Park, Y. Sidis, P. Steffens, D.L. Abernathy, P. Bourges, M. Greven, arXiv:1402.4517, 2014.
[3] W. Tabis, Y. Li, M.L. Tacon, L. Braicovich, A. Kreyssig, M. Minola, G. Dellea, E. Weschke, M.J. Veit, M. Ramazanoglu, A.I. Goldman, T. Schmitt, G. Ghiringhelli, N. Barišić, M.K. Chan, C.J. Dorow, G. Yu, X. Zhao, B. Keimer, M. Greven, arXiv:1402.7658, 2014.
[4] R.-H. He, M. Hashimoto, H. Karapetyan, J.D. Koralek, J.P. Hinton, J.P. Testaud, V. Nathan, Y. Yoshida, H. Yao, K. Tanaka, W. Meevasana, R.G. Moore, D.H. Lu, S.-K. Mo, M. Ishikado, H. Eisaki, Z. Hussain, T.P. Devereaux, S.A. Kivelson, J. Orenstein, A. Kapitulnik, Z.-X. Shen, Science 331 (6024) (2011) 1579–1583.
[5] J. Xia, E. Schemm, G. Deutscher, S.A. Kivelson, D.A. Bonn, W.N. Hardy, R. Liang, W. Siemons, G. Koster, M.M. Fejer, A. Kapitulnik, Phys. Rev. Lett. 100 (2008) 127002.
[6] Y. Okada, T. Takeuchi, T. Baba, S. Shin, H. Ikuta, J. Phys. Soc. Jpn. 77 (7) (2008) 074714.
[7] E. Pavarini, I. Dasgupta, T. Saha-Dasgupta, O. Jepsen, O.K. Andersen, Phys. Rev. Lett. 87 (2001) 047003.
[8] G. Nikšić, I. Kupčić, O.S. Barišić, D.K. Sunko, S. Barišić, J. Supercond. Novel Magn. 27 (4) (2014) 969–975.
[9] I. Kupčić, S. Barišić, Phys. Rev. B 75 (2007) 094508.
[10] J.R. Schrieffer, X.G. Wen, S.C. Zhang, Phys. Rev. B 39 (16) (1989) 11663–11679.
[11] A.V. Chubukov, D.M. Frenkel, Phys. Rev. B 46 (18) (1992) 11884–11901.
[12] I.M. Vishik, N. Barišić, M.K. Chan, Y. Li, D.D. Xia, G. Yu, X. Zhao, W.S. Lee, W. Meevasana, T.P. Devereaux, M. Greven, Z.-X. Shen, Phys. Rev. B 89 (2014) 195141.
[13] M. Matsuda, G.E. Granroth, M. Fujita, K. Yamada, J.M. Tranquada, Phys. Rev. B 87 (2013) 054508.
[14] G. Nikšić, I. Kupčić, D. Sunko, S. Barišić, J. Supercond. Nov. Magn. 26 (8) (2013) 2669–2673.